Received: 9 March 2022 | Accepted: 8 August 2022

DOI: 10.1002/hep4.2079

ORIGINAL ARTICLE

Differential expression of hepatic cancer stemness and hypoxia markers in residual cancer after locoregional therapies for hepatocellular carcinoma

Miran Kim[1] | **Kam Man Hui**[2,3,4,5] | **Ming Shi**[6] | **Nancy Reau**[1] | **Costica Aloman**[1]

[1]Division of Digestive Diseases and Nutrition, Section of Hepatology, Rush University, Chicago, Illinois, USA

[2]Department of Cellular & Molecular Research, National Cancer Center Singapore, Singapore

[3]Department of Biochemistry, Yong Loo Lin School of Medicine, National University of Singapore, Singapore

[4]Institute of Molecular and Cell Biology, A*STAR, Singapore

[5]Duke-NUS Medical School, Singapore

[6]Department of Liver Surgery, Cancer Center, Sun Yat-sen University, Guangzhou, China

Correspondence
Costica Aloman, Division of Digestive Diseases and Nutrition, Section of Hepatology, Rush University Medical Center, 1725 W. Harrison Street, Suite 319, Chicago, IL 60612, USA.
Email: costica_aloman@rush.edu

Funding information
National Institute on Alcohol Abuse and Alcoholism, Grant/Award Number: AA024762 (CA); National Medical Research Council of Singapore

Abstract

Transarterial chemoembolization (TACE) and transarterial radioembolization (TARE) treatment to hepatocellular carcinoma (HCC) are effective tools to control tumor growth, prolong survival, palliate symptoms, and improve quality of life for patients with intermediate-stage HCC. Nevertheless, there is high variability of local HCC responses to locoregional therapies; therefore, better and personalized prediction of tumor response to TACE is necessary for management of patients with HCC, especially when these modalities of treatment are used to bridge patients for liver transplant. Here, we investigated differential expression of hepatic cancer stem cell and hypoxia in residual HCC after TACE treatment in comparison with TARE. A publicly available gene data set was screened for differentially expressed genes (DEGs) in TACE_Response compared with TACE_Non-response HCC. Analysis of the GSE104580 data set displayed a total of 406 DEGs, including 196 down-regulated and 210 up-regulated DEGs. Of the 196 down-regulated DEGs, three hepatic cancer stem cell (CSC) markers and 11 hypoxia-related genes were identified. Immunohistochemical staining of hepatic CSC and hypoxia markers on explant liver tissues exhibited more intense positive staining of hepatic CSC markers (CD24, EpCAM) and hypoxia marker carbonic anhydrase 9 (CA9) in residual tumor nodule from patients with HCC treated with TACE compared with nontreated patients. Furthermore, Pearson's correlation analysis revealed the significant correlation between hepatic CSC markers and hypoxia marker, CA9. *Conclusion*: Hepatic CSC and hypoxia markers predict nonresponse to TACE and are differentially expressed in residual tumor after TACE compared with TARE. In the long term, TACE-induced hypoxia may select an aggressive HCC phenotype.

INTRODUCTION

Hepatocellular carcinoma (HCC) is a hypervascular tumor with a poor prognosis and the fourth leading cause of cancer-related mortality globally.[1,2] The incidence of HCC in the United States has more than doubled over the last 2 decades, and HCC remains difficult to manage with an overall average 5-year survival still of 18%.[1,3] For early-stage HCC treatment, liver transplant, resection, and ablation are recommended as curative therapeutic modalities. Unfortunately, a significant proportion of patients with HCC are diagnosed at intermediate or advanced stages. Currently, treatment options for these patients with intermediate and advanced HCCs remain limited to locoregional therapy (LRT), systemic chemotherapy, or more recently immunotherapy.[4–8] When there is adequate liver reserve and less aggressive biology, local advanced HCCs can be down-staged with LRT, so patients can be considered for curative treatment through liver transplant.[9] Discovery of biomarkers of tumor cell survival and aggressiveness after LRT is critical to predict, monitor, and define strategies to prevent tumor recurrence after curative treatment. For example, the presence of a hepatic cancer stem cell (CSC) gene signature that identifies the most aggressive HCC phenotype in residual HCC after LRT requires specific consideration regarding monitor of recurrence before and after liver transplant with curative intent.

Transarterial chemoembolization (TACE) is the most widely used LRT for intermediate-stage HCC.[4,5,7,8] TACE induces cancer cell death/growth arrest by inducing ischemic necrosis and increasing exposure of cancer cells to cytotoxic agents. Nonetheless, a significant number of HCCs (27%–72%) exhibit residual viable tumor after TACE.[10] Moreover, TACE-induced hypoxia in the tumor subsequently may stimulate dedifferentiation, proliferation, angiogenesis, and metastasis of the cancer itself, eventually selecting and developing an aggressive tumor phenotype (e.g., CSC class).[8,11,12] In addition, increased expression of hepatic CSC markers were found in explanted HCC after TACE treatment,[13] and this aggressive subset of HCC is induced by hypoxia.[14,15] It is unclear whether CSC/hypoxia markers found in residual tissue after TACE are the result of survival selection of any LRT or specific to TACE. Transarterial radioembolization (TARE) provides selective intra-arterial administration of microspheres loaded with a radioactive compound (usually Yttrium^{90}) and exerts its therapeutic effect through the radiation carried by these microspheres and less due to hypoxic effect.[16]

Serial imaging to monitor tumor response to LRT is the cornerstone in determining therapy efficacy. Posttreatment tumor response plays a critical role in prognosis and future treatment decision-making. However, local HCC responses to LRT are highly diverse. Even at the same Barcelona Clinical Liver Cancer stage B, different patients with HCC generally exhibit different treatment outcomes after their first LRT session.[17] Therefore, the accurate and personalized prediction of local tumor responses to the first LRT treatment holds critical clinical impact on the overall management of patients with HCC.[4,6] Current predictive models are based on clinical, radiological, and biological data. Examples include the Assessment for Retreatment with TACE score, the Selection for TACE Treatment score, the Hepatoma Arterial Embolization Prognostic score,[18–20] and functional magnetic resonance imaging technologies.[21,22] All are proposed to predict outcomes in patients with HCC undergoing TACE and are less validated in TARE. Unfortunately, these scoring systems are not widely used in clinical practice because of their disappointing accuracy.[23] Therefore, we aimed to characterize the predictive role of hepatic CSC and hypoxia markers for response of HCC to TACE treatment and validate whether there is clonal selection of these populations in comparison with the other nonhypoxic modality of LRT, TARE.

METHODS

Microarray Data collection and identification of differentially expressed genes

The GSE104580 microarray profile data set was downloaded from the Gene Expression Omnibus (GEO) database (https://www.ncbi.nlm.nih.gov/geo) to identify the differentially expressed genes (DEGs). The data set was based on the GPL570 Affymetrix Human Genome U133 Plus 2.0 Array platform (Affymetrix). The GSE104580 data set contained 81 tissue RNA samples from HCC TACE_Response patients and 66 tissue RNA samples from HCC TACE_Non-Response patients. All samples were derived from tumor biopsies of patients with HCC before TACE treatment. This study was performed as a continuing study, according to the clinical trial registered at ClinicalTrials.gov (No. NCT00493402). The evaluation of the response to TACE within 3 months (after the first or second TACE session) was assessed by extramural reviewers using the modified Response Evaluation Criteria in Solid Tumors. In this study, the tumor response was the primary endpoint of the study for final grouping. The patients with a complete response or a partial response were grouped as having an objective response to TACE, whereas patients with stable disease or progressive disease were grouped as having nonresponse to TACE. The details of the study were published previously.[24] DEGs between the two groups (TACE_Response and TACE_Non-Response) were acquired by GEO2R. To generate a

single measure of expression of genes, probe-level data were preprocessed, including background correction, normalization, and summarization, using robust multi-array average analysis adjusted for probe sequence and guanine-cytosine content. These expression measures were then log-transformed, base 2. Adjusted p value < 0.05 and |log2 fold change (FC)| > 1 were set as the cutoff criteria.

Human HCC tissue specimens

Formalin-fixed paraffin-embedded (FFPE) HCC tumor and pair-matched peritumor liver tissue sections were obtained from 15 patients who underwent liver transplant at Rush University Medical Center between July 2015 and June 2018 for a diagnosis of liver cancer after institutional review board approval and patient consent.

Immunohistochemistry

A standard immunohistochemistry (IHC) protocol was followed to stain the tumor tissue samples using antibodies against CD24 (1:100; Abcam), epithelial cell adhesion molecule (EpCAM; 1:100; Abcam), CD133 (1:50; Abcam), and carbonic anhydrase 9 (CA9; 1:250; Abcam). Briefly, 4-μm-thick FFPE sections were deparaffinized with xylene, then rehydrated through graded alcohols and subjected to antigen retrieval using a pressure cooker for 10 min in 0.01 M citrate buffer, pH 6 (ab93678; Abcam). Slides were treated with 3% H_2O_2 to quench endogenous peroxidase activity, followed by blocking with a protein block, serum-free solution (X090930-2; DAKO). After incubation with the primary antibody overnight, immunodetection was performed with Envision$^+$System-HRP Labeled Polymer Anti-mouse (K4001; DAKO) or Anti-rabbit (K4003; DAKO), followed by peroxidase-labeled streptavidin with 3,3′-diaminobenzidine (DAB) chromogen as substrate using SignalStain DAB substrate kit (8059; Cell Signaling). Slides were then counterstained with Harris Hematoxylin, mounted with SignalStain mounting medium (14177; Cell Signaling).

One-step double immunohistochemical staining of CD24 and CA9 on tumor tissue samples was performed using ImmPRESS duet double staining polymer kit (MP-7724; Vector Lab) and antibodies against CD24 (1:50, rabbit polyclonal; Abcam) and CA9 (1:200, mouse monoclonal; Abcam). In brief, FFPE sections were deparaffinized and antigen-retrieved as described previously. Slides were incubated with BLOXALL blocking solution (Vector lab) for 10 min to quench endogenous peroxidase activity, followed by blocking with a protein block, serum-free solution (DAKO). Slides were incubated with mixture of primary antibodies overnight at 4°C. As controls, antibody against CD9 or CD24 was incubated as single staining. ImmPRESS Duet Reagent containing horseradish peroxidase (HRP) horse anti-rabbit immunoglobulin G (IgG) and alkaline phosphatase horse anti-mouse IgG was incubated for 20 min, followed by two-step substrate development. At first, ImmPACT DAB EqV substrate to detect CA9 was applied for 2 min. After washed the slide, ImmPACT Vector Red substrate to detect CD24 was incubated for 20 min. Slides were counterstained with Hematoxylin QS counterstain (H-3404; Vector Lab) and mounted with VectaMount Express mounting medium (H-5700; Vector Lab).

Quantitative analysis of IHC staining

Images of DAB staining were examined using a Leica DM light microscope equipped with a SPOT Insight 4 MP Color Mosaic camera (Diagnostic Instruments, Inc.) and SPOT Software (Ver 4.6, SPOT Imaging). To minimize the selection bias of microscopic sections, 15–20 non-overlapping, randomly selected fields were captures from each slide at ×10 and ×40.

Quantification of DAB-positive regions was performed using ×10 images and the Fiji program (Image J; National Institutes of Health). Customized evaluation protocols were optimized. In brief, digital images were imported as image sequence, followed by the spectral deconvolution method of DAB/hematoxylin color spectra for proper separation of the DAB color spectra. The threshold for positive staining was set and subsequently batch-processed to minimize technical variation or potential bias. The positive staining intensity was scored as Integrated Density (IntDen), which sums all the pixels within the area and gives a total value within the threshold. Average IntDen value of each slide was calculated from 15–20 images.

Tumor nodule and stromal regions were annotated manually based on morphology, and the boundary was marked between the two regions. The marked images were used to generate either nodule or stroma-only images by Photoshop, followed by quantitation of the positive staining.

Statistical analysis

GraphPad Prism version 8.3 (GraphPad Software, Inc.) was used for all statistical analyses. Two-way analysis of variance followed by Tukey's multiple comparisons test was used to compare two variables in more than two groups. Correlation between CSC markers as well as between CA9 and CSC markers were analyzed using Pearson's correlation. Asterisks indicate levels of significance as follows: *p < 0.05, **p < 0.01, ***p < 0.001, and ****p < 0.0001. Data are presented as means ± SEM.

RESULTS

Expression profiles of DEGs between TACE_Response and TACE_Non-Response HCC samples

The GSE104580 microarray profile data set, which included a total of 147 tissue RNA samples derived from tumor biopsies of patients with HCC before TACE treatment (81 TACE_Response and 66 TACE_Non-response), was obtained from the GEO database to identify the DEGs. GEO2R was used to identify DEGs between TACE_Response and TACE_Non-Response HCC samples, with adjusted $p < 0.05$ and |log2FC| >1 set as the cutoff criteria. We identified a total of 406 DEGs, including 196 down-regulated and 210 up-regulated DEGs (Tables S1 and S2, Figure 1A). Of the 196 down-regulated DEGs, 3 genes are known as hepatic CSC markers,[25–33] including CD24, EpCAM, and alpha-fetoprotein (AFP) (Figure 1A,B). In addition, 11 hypoxia-related genes including CA9, N-myc downstream regulated 1, solute carrier family 2 member 1, hypoxia inducible lipid droplet associated, hexokinase 2, enolase 2, CD24, BMP and activin membrane bound inhibitor, adrenomedullin, serine peptidase inhibitor, Kazal type 1, secreted phosphoprotein 1, and egl-9 family hypoxia inducible factor 3 were found to be down-regulated (Figure 1A,C). Of note, CD24 is known as a hepatic CSC marker as well as hypoxia-regulated gene. These findings suggest that levels of hepatic CSC markers as well as hypoxic markers might be associated with HCC response to TACE.

Clinical characteristics of the patients

To further confirm that the expression profile of hepatic CSC and hypoxia markers are associated with residual HCC after TACE, we used liver explant tissue sections obtained from 15 patients who underwent liver transplant for liver cancer. Treated patients in this set of tissue samples could have had either TACE or TARE; none of the patients included in the study had combined modalities of LRT treatment. As controls, we included TARE-treated patients with HCC as a nonhypoxic approach to treat HCC as well as completely nontreated patients with HCC. TARE is considered second-line treatment for intermediate-stage HCC.[7,8] Unlike TACE treatment, the antitumor effect of TARE is due to β-radiation cytotoxicity and has minimal vascular ischemic effect. If treatment-associated hypoxia with TACE changes tumor biology, TARE should be a superior modality, as the antitumor effect is not hypoxic-mediated.

The overall demographic and clinical characteristics of the patients with HCC, including TACE-treated (n = 7), TARE-treated (n = 4), and nontreated (n = 4), are summarized in Table 1. The mean ages of TACE-treated, TARE-treated, and nontreated were 64.29 ± 3.50, 64.50 ± 4.36, and 57.25 ± 8.18 years, respectively. The mean Model for End-Stage Liver Disease (MELD) score of TACE-treated, TARE-treated, and nontreated was 18.71 ± 10.78, 12.00 ± 2.45, and 32.25 ± 13.05, respectively. The difference in MELD score, MELD-Na score, and AFP value between total treated (LRT) and nontreated was significant ($p = 0.0241$, $p = 0.0325$, and $p = 0.0249$, respectively), as expected, considering that patients with poor hepatic reserve are not able to get LRT (Figure S1).

Immuno-profiles of hepatic CSC markers and hypoxia markers in different LRT types of HCC

The biological behavior of tumors and tumor progression are known to be affected not only by the tumor cells themselves but also deeply influenced by their interactions with the adjacent stroma.[12,34–37] This tumor-stroma crosstalk is enhanced by hypoxia.[38] Furthermore, a growing body of evidence suggests that late recurrence and poor clinical outcome have been associated with the gene-expression signature of nontumoral liver tissue adjacent to the primary tumor.[12,39,40] More importantly, hepatic CSCs,

FIGURE 1 Down-regulated genes related hepatic cancer stem cell and hypoxia in samples derived from TACE_response patients with hepatocellular carcinoma (HCC). Differentially expressed genes (DEGs) between the two groups (TACE_Response and TACE_Non-Response) were acquired by GEO2R. (A) Volcano plot depicts DEGs between TACE_Response and TACE_Non-response. Volcano map displayed 210 up-regulated and 196 down-regulated DEGs in TACE_Response group compared with TACE_Non-response group. Adjusted p value < 0.05 and |log2 fold change (FC)| > 1 were set as the cutoff criteria. Blue dots, down-regulated genes; red dots, up-regulated genes. (B,C) Expression levels of hepatic cancer stem markers (B) and hypoxia-related genes (C) depicted as violin plots. Expression levels were acquired from GSE104580. Data were preprocessed, including background correction, normalization, and summarization, using robust multi-array average (RMA) analysis adjusted for probe sequence and guanine-cytosine content (GCRMA). These expression measures were then log-transformed, base 2 (log 2 GCRMA). Violin plots show the median (red solid line) and quartiles (dotted line) from TACE_Non-response (n = 66) and TACE_Response (n = 81). Statistically significant differences are indicated as $^{**}p < 0.01$, $^{***}p < 0.001$, and $^{****}p < 0.0001$. ADM, adrenomedullin; AFP, alpha-fetoprotein; BAMBI, BMP and activin membrane bound inhibitor; CA9, carbonic anhydrase 9; EGLN3, egl-9 family hypoxia inducible factor 3; ENO2, enolase 2; EpCAM, epithelial cell adhesion molecule; HILPDA, hypoxia inducible lipid droplet associated; HK2, hexokinase 2; NDGR1, N-myc downstream regulated 1; SLC2A1, solute carrier family 2 member 1; SPINK1, serine peptidase inhibitor, Kazal type 1; SPP1, secreted phosphoprotein 1; TACE, transarterial chemoembolization.

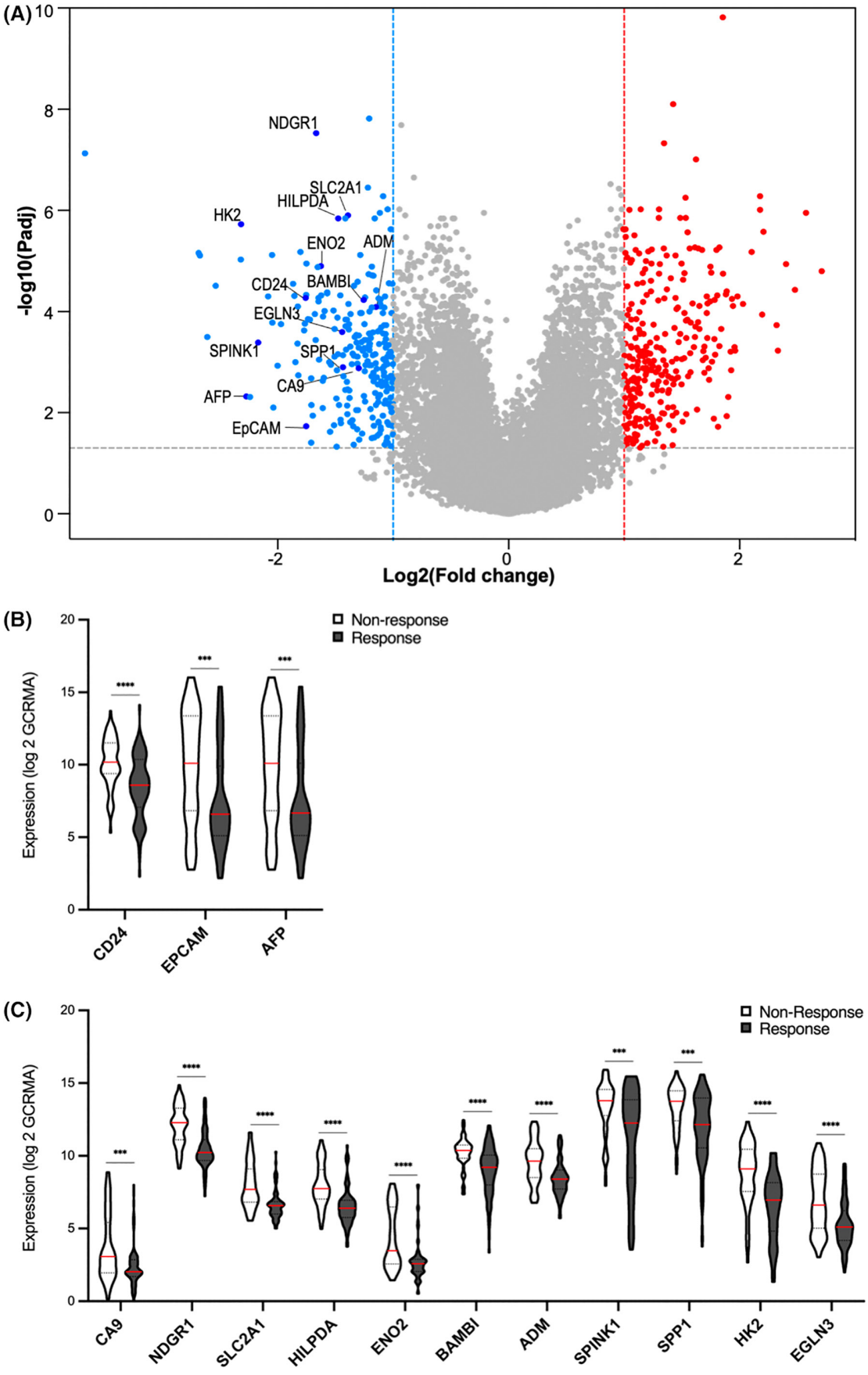
(A)
-log10(Padj)
Log2(Fold change)
NDGR1
SLC2A1
HILPDA
HK2
ENO2
ADM
CD24
BAMBI
EGLN3
SPINK1
SPP1
CA9
AFP
EpCAM
(B)
Non-response
Response
Expression (log 2 GCRMA)
CD24
EPCAM
AFP
(C)
Non-Response
Response
Expression (log 2 GCRMA)
CA9
NDGR1
SLC2A1
HILPDA
ENO2
BAMBI
ADM
SPINK1
SPP1
HK2
EGLN3

TABLE 1 Clinicopathological features of HCCs in the locoregional therapy (TACE and TARE) and NT group

Parameters	Locoregional therapy		NT (n = 4)	*p* value[b]
	TACE (n = 7)	TARE (n = 4)		
Age (years)	64.29 ± 3.50	64.50 ± 4.36	57.25 ± 8.18	0.4348
Gender (male/female, %)	5/2, 71	3/1, 75	1/4, 25	n.a.
Etiology (HBV/HCV/alcohol/other)	1/0/4/2	1/0/0/3	0/0/1/3	n.a.
MELD	18.71 ± 10.78	12.00 ± 2.45	32.25 ± 13.05	0.0241
MELD-Na	20.00 ± 11.06	13.25 ± 2.36	32.75 ± 12.50	0.0325
Serum AFP (IU/L)	3.81 ± 5.13	7.07 ± 3.81	52.55 ± 60.97	0.0249
AFP producer (%)	14.2	50	75	n.a.

Note: Data were collected at liver transplant and are presented as mean value ± SD or counts (%).

Abbreviations: HBV, hepatitis B virus; HCV, hepatitis C virus; LRT, locoregional therapy; MELD, Model for End-Stage Liver Disease; n.a., not applicable.

[b]*p* value of total treated (LRT) versus nontreated.

which contribute to an aggressive biological behavior, are also affected by the tumor stroma.[41] Thus, we evaluated the expression of CSC markers and hypoxia markers in both tumor nodule and stroma, to determine whether there was differential expression of these markers depending on the type of LRT. Furthermore, we sought to assess hepatic CSC markers as well as hypoxic markers in HCC tumor and pair-matched peritumor liver-tissue sections obtained from liver explants.

Expression patterns of hepatic CSC markers (CD24, EpCAM, and CD133) were determined by IHC staining in samples of TACE-T (tumor from TACE-treated HCC), TARE-T (tumor from TARE-treated HCC), and NT-T (tumor from nontreated HCC) as well as TACE-pT (a pair-matched adjacent peritumor from TACE-treated HCC), TARE-pT (a pair-matched adjacent peritumor from TARE-treated HCC), and NT-pT (a pair-matched adjacent peritumor from nontreated HCC).

CD24 expression was significantly up-regulated in residual TACE-T compared with TARE-T and NT-T ($p < 0.01$ and $p < 0.01$, respectively) (Figure 2A). In TACE-treated HCC, TACE-T showed a significantly higher level of CD24 than TACE-pT ($p < 0.05$) (Figure 2A). Strong cytoplasmic and membranous staining pattern was observed in tumor nodules (Figure S2A). Furthermore, CD24 positivity was detected stronger in the edge of large tumor nodules close to thick fibrous bands (Figure S2A, arrows). In addition, biliary epithelium cells (Figure S2A, arrowheads), bile canaliculi (Figure S2B, arrows), ductules (Figure S2B, arrowheads), ductular hepatocytes (Figure S2C, arrows), and lymphocytic inflammatory infiltrates (Figure S2D, arrow) displayed CD24 positivity.

EpCAM was also significantly overexpressed in residual TACE-T compared with TARE-T and NT-T ($p < 0.001$ and $p < 0.01$, respectively) (Figure 2B). Expression of EpCAM in TACE-T was significantly higher than TACE-pT as well ($p < 0.01$) (Figure 2B). EpCAM expression pattern showed diffuse positive staining (cytoplasmic and membranous pattern) with variable staining distribution (Figure 2B, Figure S3). Like earlier studies, strong staining of EpCAM in the bile ducts was found (Figure S3A, arrows). We also noticed that EpCAM was expressed in ductules and ductular hepatocytes (Figure S3B, arrows) as well as scirrhous pattern tumor cells, which embedded in loose, myxoid stroma (Figure S3C, arrows).

Expression level of CD133 in TACE-T was higher than TACE-pT but did not reach a significant difference. There were also no significant differences among TACE-T, TARE-T, and NT-T (Figure 2C). It is noticeable that CD133, unlike CD24 and EpCAM, was not found as one of the DEGs between TACE_Response and TACE_Non-Response HCC samples in the GSE data set. CD133 expression exhibited a diffuse staining pattern as cytoplasmic and membranous of tumor cells (Figure S4). Of note, CD133 membranous staining was limited to apical membrane of tumor cells facing lumen of bile canaliculi, not basolateral membrane facing sinusoids (Figure S4A, arrows). This observation is consistent with a report that CD133 has a remarkable subcellular localization, exclusively located in apical-specific localization, which prevent the lateral diffusion of apical transmembrane proteins into the lateral plasma membrane.[42,43] Furthermore, studies demonstrated that the surface area of the canalicular membrane showed dramatical increase of microvilli in which CD133 is selectively localized.[42,44] In addition, bile ducts revealed strong expression (Figure S4B, arrow) as previously reported.[45] Rosette-like structure created by a bile canaliculus surrounded by hepatocytes also expressed CD133 (Figure S4C, arrows).

Next, the comparison of expression of hepatic CSC markers between tumor nodule and stroma was addressed. To analyze tumor nodule and tumor stroma independently, we generated either nodule-only or stroma-only IHC images by Photoshop (Figures S5 and S6). The significant increase of CD24 and EpCAM expression occurred in the tumor nodules of TACE-T compared with those of TARE-T and NT-T, not in the

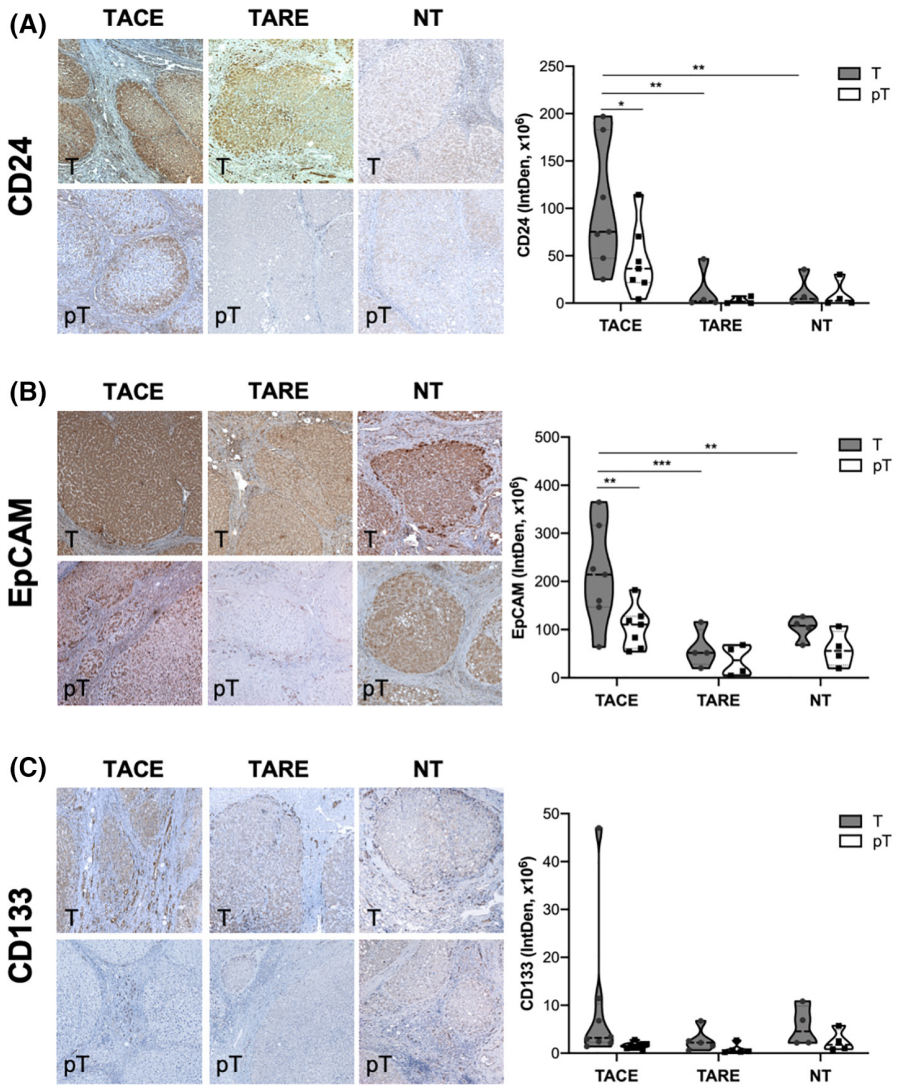

FIGURE 2 Expression of hepatic CSC markers in tumor from TACE-treated patients with HCC compared with TARE or nontreated patients. Formalin-fixed paraffin-embedded (FFPE) liver explant specimens from patients were subjected to immunohistochemical (IHC) staining for detection of hepatic cancer stem cell (CSC) markers. Representative positive IHC image (×10) and a violin plot showing Integrated Density of CD24 (A), EpCAM (B), and CD133 (C) from TACE, transarterial radioembolization (TARE), and nontreated (NT). Intensity of the positive staining of tumor and pair-matched adjacent peritumor samples was determined by Fiji (Image J) and presented as Integrated Density (IntDen). The data represent the mean ± SEM, TACE (n = 7), TARE (n = 4), and NT (n = 4). Statistically significant differences are indicated as determined by two-way analysis of variance (ANOVA) (*$p < 0.05$, **$p < 0.01$, and ***$p < 0.001$). pT, peritumor; T, tumor.

stroma (Figure 3A,B). Furthermore, in TACE-T, CD24, and EpCAM expression was higher in nodule than stroma (Figure 3A,B).

Herein, we demonstrated that CD24 and EpCAM expression in the residual HCC after TACE-T is consistently strong among all groups we tested (Figure 3).

Hepatic hypoxia marker CA9 expression was significantly up-regulated in TACE-T compared with TARE-T and NT-T ($p < 0.05$ and $p < 0.05$, respectively) as well as compared with TACE-pT ($p < 0.01$) (Figure 4A). As shown in Figure 4B, the status of CA9 expression in the nodule of TACE-T was higher than those of TARE-T ($p < 0.01$). Interestingly, CA9 expression was higher in the stroma of TACE-T compared with those of NT-T ($p < 0.05$).

The CA9 staining displayed heterogeneous and diffuse membranous/cytoplasmic staining, with areas of concurrent cytoplasmic and nuclear staining (Figure S7A). In addition, ductular hepatocytes (Figure S7B, arrows) and ductules (Figure S7C, arrows) showed the CA9 positivity. The periphery of necrotic tumor tissue (*N*) exhibited strong CA9 expression (Figure S7C, arrowheads).

Finally, we explored whether there is any correlation between different hepatic CSC marker expression as well as CA9. The degree of CD24 expression was well correlated with CD133 and EpCAM ($p < 0.0001$ and $p < 0.0001$, respectively), but not between CD133 and EpCAM expression ($p = 0.1294$) (Figure 5A). The

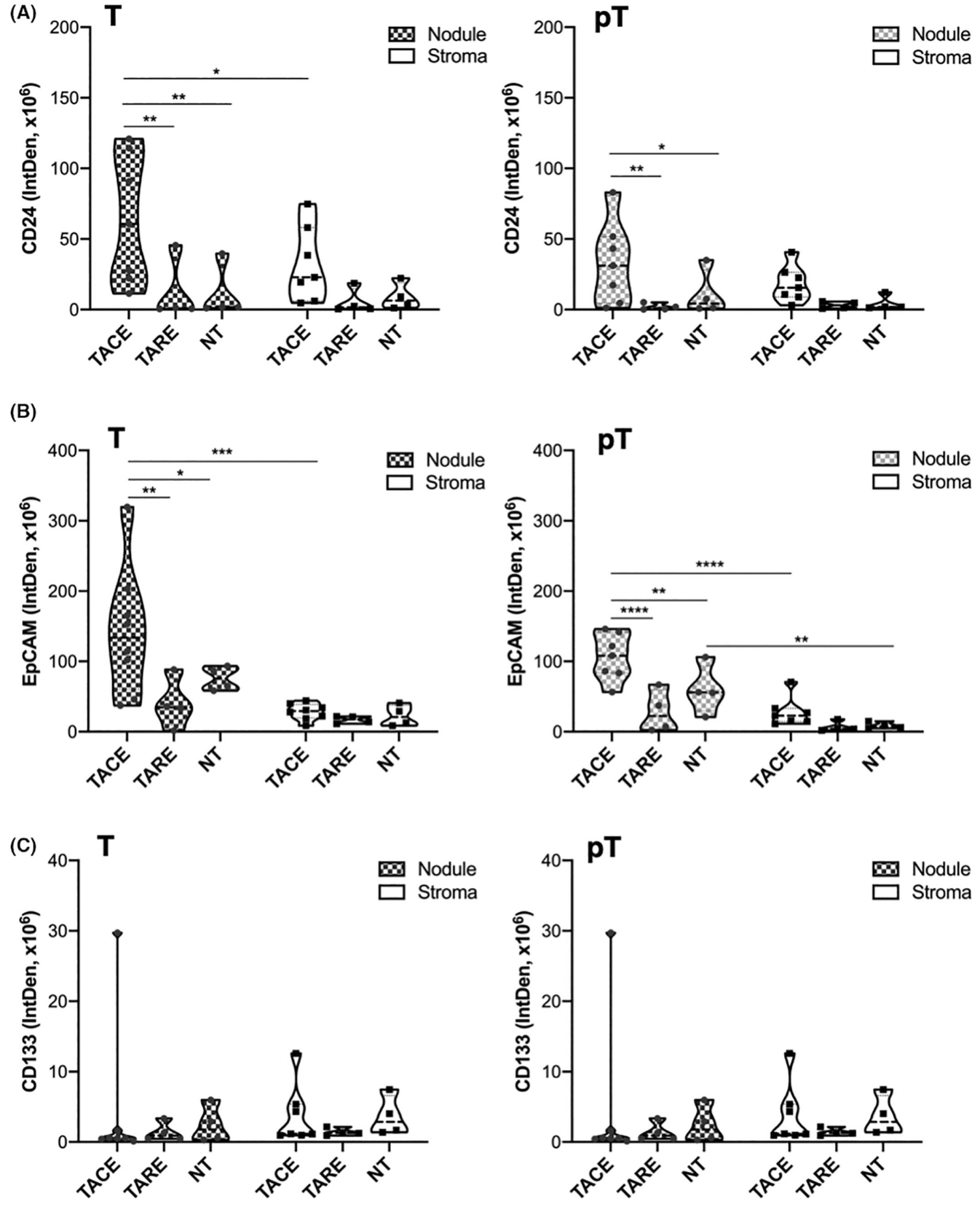

FIGURE 3 Expression of CSC markers in tumor nodule and stroma from TACE-treated patients with HCC compared with TARE or nontreated patients. Intensity of positive staining of CD24 (A), EpCAM (B), and CD133 (C) from either nodule or stroma in tumor and peritumor samples. Both nodule-only and stroma-only digital images were obtained using Photoshop. Intensity of the positive staining was determined by Fiji (Image J) and presented as IntDen. The data represent the mean ± SEM, TACE (n = 7), TARE (n = 4), and NT (n = 4). Statistically significant differences are indicated as determined by two-way ANOVA (*$p < 0.05$, **$p < 0.01$, and ***$p < 0.001$).

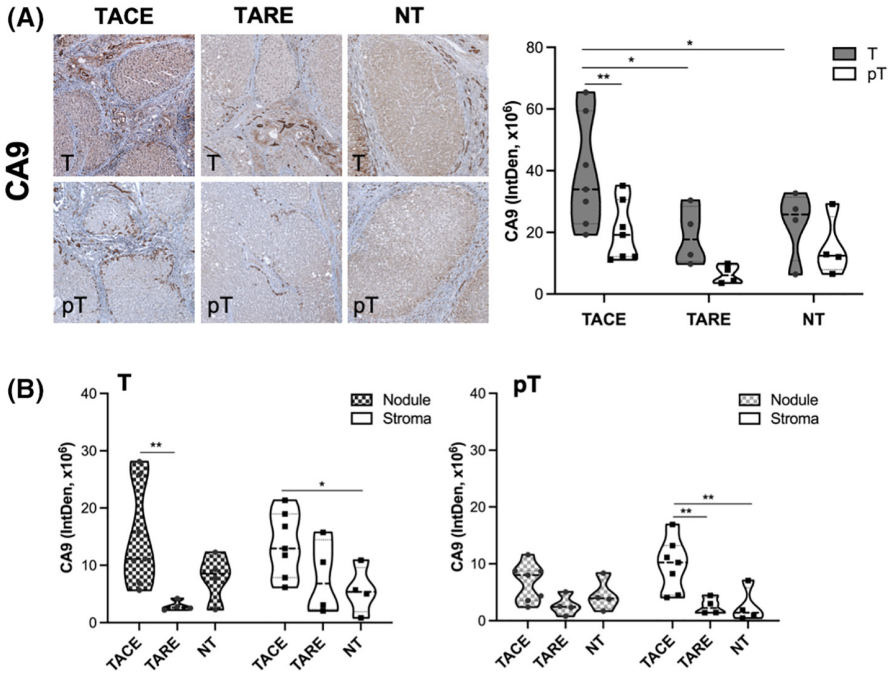

FIGURE 4 CA9 expression increased in tumor from TACE-treated patients with HCC compared with TARE or NT patients. FFPE liver explant specimens from patients were subjected to IHC staining for detection of CA9 expression. (A) Representative positive IHC image (×10) of CA9 and a violin plot showing IntDen of CA9 expression from TACE, TARE, and NT. Intensity of the positive staining of tumor and peritumor samples was determined by Fiji (Image J) and presented as IntDen. (B) Intensity of positive staining from either nodule or stroma in tumor and peritumor samples. Both nodule-only and stroma-only images were prepared using Photoshop followed by analysis of IntDen. The data represent the mean ± SEM, TACE (n = 7), TARE (n = 4), and NT (n = 4). Statistically significant differences are indicated as determined by two-way ANOVA (*$p < 0.05$ and **$p < 0.01$).

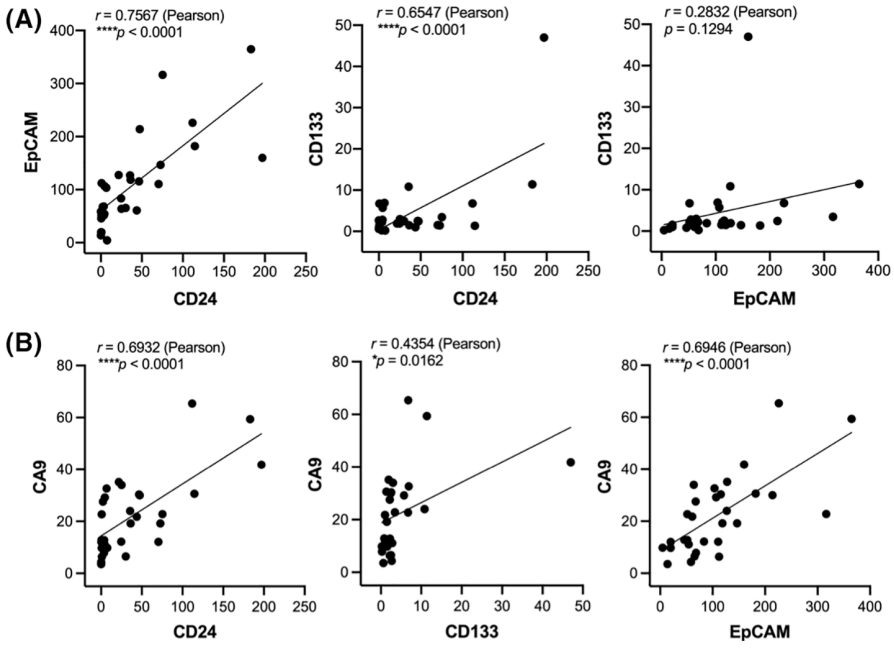

FIGURE 5 Correlation between hepatic CSC markers and CA9. Pearson's correlation test was applied between hepatic CSC markers (A) and between CA9 and hepatic CSC markers (B). Expression of hepatic CSC markers is positively correlated with hypoxia marker (CA9). (C,D) Double IHC staining of CA9 and CD24 in TACE-T (tumor from TACE-treated HCC (C) and TARE-T (tumor from TARE-treated HCC) (D) samples. FFPE liver explant specimens from patients were subjected to double IHC staining for co-expression of CA9 and CD24. Single IHC staining of CA9 and CD24 served as controls. Representative CA9 staining (left panels), CD24 staining (middle panels), and double-positive IHC images of CA9 and CD24 (right panels) are depicted. Bottom panels (×40) are the boxed area of the top panels. In (D), CA9 single positive cells (brown arrows), CD24 single positive cells (magenta arrows), and double positive of CA9 and CD24 cells (yellow arrows) are displayed.

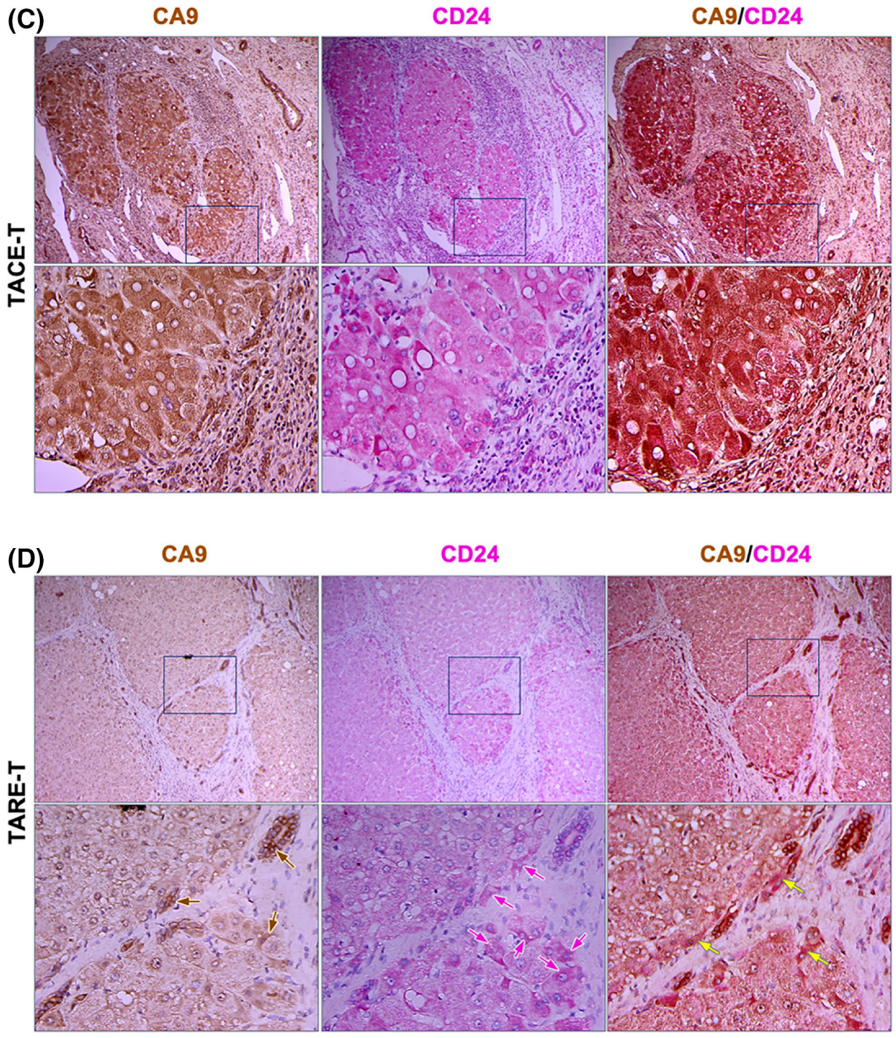

FIGURE 5 (Continued)

degree of hypoxia marker CA9 expression was significantly correlated with all hepatic CSC markers of CD24, CD133, and EpCAM ($p < 0.0001$, $p = 0.0162$, and $p < 0.0001$, respectively) (Figure 5B). To further establish the relationship between CA9 and CD24 expression in hypoxic tumor microenvironment, double IHC staining of CA9 and CD24 was performed in TACE-T and TARE-T samples. Robust positive double-staining of CA9 and CD24 was found in most tumor cells, ductules, and ductular hepatocytes in TACE-T samples (Figure 5C, right panels). On the other hand, only a few cells at the edge of large tumor nodules exhibited weak positive double-staining of CA9 and CD24 (Figure 5D, right panels, yellow arrows). CA9 single positive staining was positive in ductules (Figure 5D, left panels, brown arrows), and a few tumor cells at the edge of large tumor nodules exhibited CD24 single positive staining (Figure 5D, middle panels, magenta arrows). Although double-staining of CA9 and CD24 positive tumor cells were detected in both TACE-T and TARE-T samples, the intensity of positive staining as well as the number of positive cells are more potent in TACE-T, demonstrating the tight relationship between CD24 (hepatic CSC marker) and CA9 (hypoxia marker) in the TACE-induced hypoxic tumor microenvironment.

DISCUSSION

Our study showed that pretreatment tissue expression of both hepatic CSC markers and hypoxia markers transcripts correlate with response to TACE treatment in patients with HCC by GSE data-set analysis. Furthermore, the residual tumor nodules after TACE treatment also exhibited high level of hepatic CSC markers and hypoxia markers compared with TARE treatment by IHC staining.

Recently, two papers have described gene signatures to predict the response to TACE in patients with HCC.[46,47] Fako et al. reported TACE-specific 14-gene signature as TACE Navigator, which was associated with improved survival in patients who received either adjuvant or postrelapse TACE. It was suggested that hypoxia response may be linked to TACE treatment

resistance based on up-regulation of hypoxia inducible factor 1 alpha subunit and vascular endothelial growth factor in nonresponders compared with responders. Nevertheless, both genes are not included in the gene signature. Another report identified a 10-gene signature from the GSE104580 data set using machine learning–based gene selection. In this manuscript, it is proposed that stemness index is higher in nonresponder compared with responder, although neither stemness marker nor hepatic CSC marker are included in the 10-gene signature. Despite the fact that both studies define TACE-specific response gene signatures in patients with HCC, no gene overlap is common in both studies. It is noteworthy that our data showed that both hepatic CSC markers and hypoxia markers are identified as enriched in residual HCC after TACE. These differences in conclusions may be the result of our comparison that has been made not only by using the public GSE data set but also by using control samples from patients treated with a non-hypoxic-mediated LRT (TARE). Moreover, our study provides descriptive information regarding the effect of LRT on peritumoral tissue in patients with residual HCC.

IHC serves as a diagnostic and prognostic method for identification of various disease markers in human tissue samples that directly influence classification and grading the disease. Despite the potential impact on prognosis and management, their role in patient management remains limited. However, most pathological analysis of tissue samples is carried out in a time-consuming and subjective manner, wherein the intensity of antibody staining is manually judged and thus scoring decisions are directly determined by a visual bias. In this study, quantitative assessment of antibody staining intensity in human tissue sections was performed by automated digital IHC image analysis using Fiji program (Image J). We captured and used 15–20 nonoverlapping, randomly selected digital images from each slide to minimize the selection bias of microscopic sections. As a readout of the positive staining intensity, IntDen, which gives a total value within the threshold, was used. This analytical method minimized interobserver as well as interslide variations.

Ductular reaction (DR) is known to be present in most chronic liver diseases and is also important in hepatic stem and progenitor cell liver regeneration mechanisms, which underlie hepatic fibrosis and hepatobiliary carcinogenesis. Peritumoral DRs correlate with intratumoral hepatic progenitor cell (HPC) markers EpCAM, OV6, and CD133 expression.[48] Studies showed an extensive DR in advanced HCC and a strong correlation between cytokeratin 7 expression and the poor prognosis and aggressiveness of HCC.[49] In our data, strong expression of both hepatic CSC markers (CD24 and EpCAM) and hypoxia marker (CA9) was detected in DR cells. We speculated that hypoxia might be involved in proliferative DRs, eventually contributing to the development of an aggressive HCC phenotype. Further work will be required to determine the precise cellular mechanism mediated by hypoxia-driven DR that render HPC to hepatic CSCs.

One previous study indicated that the location of CD133 on the CSC may play an important role on the aggressiveness of the cancer and the prognosis of the liver cancer patient. They reported that cytoplasmic CD133 expression was correlated with poor prognosis, whereas nuclear CD133 expression was correlated with favorable prognosis.[50] In the present study, distinctive membranous staining pattern of CD133 was found.

This study presents quantitation of IHC to define immune profiling of CSC markers in both tumor nodule and stroma in detail using specimens from TACE, TARE, and nontreated patients with HCC. Limitations of this study include a single-center study and the relatively small sample size. Further studies based on a larger number of cases from multiple centers will be required. In addition, more CSC and hypoxia markers should be tested, as only a few CSC markers and hypoxia markers were included in this study.

CONCLUSIONS

The expression of hepatic CSC markers is increased primarily in residual tumor nodule under TACE-induced hypoxia, which might promote the aggressive biology of HCC as well as unlikely response to TACE treatment based on GSE data-set analysis. Therefore, examining the expression status of these markers in biopsied HCCs may facilitate clinical decision making and could potentially help to predict a poor outcome of HCCs, and thereby further guide treatment planning and surveillance after resection or liver transplant. Moreover, it will support a paradigm shift in intermediate HCC management in which usually tissue sampling is rarely required.

AUTHOR CONTRIBUTIONS

Experiment design: Miran Kim and Costica Aloman. *Data acquisition*: Miran Kim, Kam Man Hui, and Ming Shi. *Analysis*: Miran Kim. *Data interpretation*: Miran Kim, Kam Man Hui, and Ming Shi. *Statistical analysis*: Miran Kim. *Manuscript draft*: Miran Kim. *Critical revision of the manuscript*: Kam Man Hui, Ming Shi, Nancy Reau, and Costica Aloman. *Study supervision and funding obtainment*: Costica Aloman. All authors approved the final version of the manuscript.

FUNDING INFORMATION

Supported by the National Institutes of Health (Grant No. 2017, AA024762) and the National Medical Research Council of Singapore.

CONFLICT OF INTEREST

Nothing to report.

ORCID

Ming Shi https://orcid.org/0000-0002-4051-4474
Costica Aloman https://orcid.org/0000-0002-2888-1984

REFERENCES

1. Kim HS, El-Serag HB. The epidemiology of hepatocellular carcinoma in the USA. Curr Gastroenterol Rep. 2019;21:17.
2. Couri T, Pillai A. Goals and targets for personalized therapy for HCC. Hepatol Int. 2019;13:125–37.
3. Villanueva A. Hepatocellular carcinoma. N Engl J Med. 2019;380:1450–62.
4. EASL Clinical Practice Guidelines: management of hepatocellular carcinoma. J Hepatol. 2018;69:182–236.
5. Heimbach JK, Kulik LM, Finn RS, Sirlin CB, Abecassis MM, Roberts LR, et al. AASLD guidelines for the treatment of hepatocellular carcinoma. Hepatology. 2018;67:358–80.
6. Piscaglia F, Ogasawara S. Patient selection for transarterial chemoembolization in hepatocellular carcinoma: importance of benefit/risk assessment. Liver Cancer. 2018;7:104–19.
7. Marrero JA, Kulik LM, Sirlin CB, Zhu AX, Finn RS, Abecassis MM, et al. Diagnosis, staging, and management of hepatocellular carcinoma: 2018 Practice Guidance by the American Association for the Study of Liver Diseases. Hepatology. 2018;68:723–50.
8. Sangro B, Salem R. Transarterial chemoembolization and radioembolization. Semin Liver Dis. 2014;34:435–43.
9. Kollmann D, Selzner N, Selzner M. Bridging to liver transplantation in HCC patients. Langenbecks Arch Surg. 2017;402:863–71.
10. Chua TC, Liauw W, Saxena A, Chu F, Glenn D, Chai A, et al. Systematic review of neoadjuvant transarterial chemoembolization for resectable hepatocellular carcinoma. Liver Int. 2010;30:166–74.
11. Rhee H, Nahm JH, Kim H, Choi GH, Yoo JE, Lee HS, et al. Poor outcome of hepatocellular carcinoma with stemness marker under hypoxia: resistance to transarterial chemoembolization. Mod Pathol. 2016;29:1038–49.
12. Rhee H, Chung T, Yoo JE, Nahm JH, Woo HY, Choi GH, et al. Gross type of hepatocellular carcinoma reflects the tumor hypoxia, fibrosis, and stemness-related marker expression. Hepatol Int. 2020;14:239–48.
13. Zeng Z, Ren J, O'Neil M, Zhao J, Bridges B, Cox J, et al. Impact of stem cell marker expression on recurrence of TACE-treated hepatocellular carcinoma post liver transplantation. BMC Cancer. 2012;12:584.
14. Fujikuni N, Yamamoto H, Tanabe K, Naito Y, Sakamoto N, Tanaka Y, et al. Hypoxia-mediated CD24 expression is correlated with gastric cancer aggressiveness by promoting cell migration and invasion. Cancer Sci. 2014;105:1411–20.
15. Tomimaru Y, Koga H, Yano H, de la Monte S, Wands JR, Kim M. Upregulation of T-cell factor-4 isoform-responsive target genes in hepatocellular carcinoma. Liver Int. 2013;33:1100–12.
16. Sacco R, Mismas V, Marceglia S, Romano A, Giacomelli L, Bertini M, et al. Transarterial radioembolization for hepatocellular carcinoma: an update and perspectives. World J Gastroenterol. 2015;21:6518–25.
17. Lencioni R, de Baere T, Soulen MC, Rilling WS, Geschwind JF. Lipiodol transarterial chemoembolization for hepatocellular carcinoma: a systematic review of efficacy and safety data. Hepatology. 2016;64:106–16.
18. Hucke F, Pinter M, Graziadei I, Bota S, Vogel W, Müller C, et al. How to STATE suitability and START transarterial chemoembolization in patients with intermediate stage hepatocellular carcinoma. J Hepatol. 2014;61:1287–96.
19. Sieghart W, Hucke F, Pinter M, Graziadei I, Vogel W, Müller C, et al. The ART of decision making: retreatment with transarterial chemoembolization in patients with hepatocellular carcinoma. Hepatology. 2013;57:2261–73.
20. Kadalayil L, Benini R, Pallan L, O'Beirne J, Marelli L, Yu D, et al. A simple prognostic scoring system for patients receiving transarterial embolisation for hepatocellular cancer. Ann Oncol. 2013;24:2565–70.
21. Abajian A, Murali N, Savic LJ, Laage-Gaupp FM, Nezami N, Duncan JS, et al. Predicting treatment response to intraarterial therapies for hepatocellular carcinoma with the use of supervised machine learning-an artificial intelligence concept. J Vasc Interv Radiol. 2018;29:850–7.e851.
22. Thibodeau-Antonacci A, Petitclerc L, Gilbert G, Bilodeau L, Olivié D, et al. Dynamic contrast-enhanced MRI to assess hepatocellular carcinoma response to transarterial chemoembolization using LI-RADS criteria: a pilot study. Magn Reson Imaging. 2019;62:78–86.
23. Mähringer-Kunz A, Wagner F, Hahn F, Weinmann A, Brodehl S, Schotten S, et al. Predicting survival after transarterial chemoembolization for hepatocellular carcinoma using a neural network: a Pilot Study. Liver Int. 2020;40:694–703.
24. Shi M, Lu LG, Fang WQ, Guo RP, Chen MS, Li Y, et al. Roles played by chemolipiodolization and embolization in chemoembolization for hepatocellular carcinoma: single-blind, randomized trial. J Natl Cancer Inst. 2013;105:59–68.
25. Suetsugu A, Nagaki M, Aoki H, Motohashi T, Kunisada T, Moriwaki H. Characterization of $CD133^+$ hepatocellular carcinoma cells as cancer stem/progenitor cells. Biochem Biophys Res Commun. 2006;351:820–4.
26. Ma S, Chan KW, Hu L, Lee TK, Wo JY, Ng IO, et al. Identification and characterization of tumorigenic liver cancer stem/progenitor cells. Gastroenterology. 2007;132:2542–56.
27. Yang ZF, Ho DW, Ng MN, Lau CK, Yu WC, Ngai P, et al. Significance of CD90+ cancer stem cells in human liver cancer. Cancer Cell. 2008;13:153–66.
28. Zhu Z, Hao X, Yan M, Yao M, Ge C, Gu J, et al. Cancer stem/progenitor cells are highly enriched in $CD133^+CD44^+$ population in hepatocellular carcinoma. Int J Cancer. 2010;126:2067–78.
29. Yamashita T, Ji J, Budhu A, Forgues M, Yang W, Wang HY, et al. EpCAM-positive hepatocellular carcinoma cells are tumor-initiating cells with stem/progenitor cell features. Gastroenterology. 2009;136:1012–24.
30. Yang W, Wang C, Lin Y, Liu Q, Yu LX, Tang L, et al. $OV6^+$ tumor-initiating cells contribute to tumor progression and invasion in human hepatocellular carcinoma. J Hepatol. 2012;57:613–20.
31. Haraguchi N, Ishii H, Mimori K, Tanaka F, Ohkuma M, Kim HM, et al. CD13 is a therapeutic target in human liver cancer stem cells. J Clin Invest. 2010;120:3326–39.
32. Lee TK, Castilho A, Cheung VC, Tang KH, Ma S, Ng IO. CD24(+) liver tumor-initiating cells drive self-renewal and tumor initiation through STAT3-mediated NANOG regulation. Cell Stem Cell. 2011;9:50–63.
33. Liu C, Liu L, Chen X, Cheng J, Zhang H, Shen J, et al. Sox9 regulates self-renewal and tumorigenicity by promoting symmetrical cell division of cancer stem cells in hepatocellular carcinoma. Hepatology. 2016;64:117–29.
34. Hwang RF, Moore T, Arumugam T, Ramachandran V, Amos KD, Rivera A, et al. Cancer-associated stromal fibroblasts promote pancreatic tumor progression. Cancer Res. 2008;68:918–26.
35. Allen M, Louise Jones J. Jekyll and Hyde: the role of the microenvironment on the progression of cancer. J Pathol. 2011;223:162–76.
36. Jing Y, Han Z, Zhang S, Liu Y, Wei L. Epithelial-mesenchymal transition in tumor microenvironment. Cell Biosci. 2011;1:29.
37. Eiró N, Vizoso FJ. Importance of tumor/stroma interactions in prognosis of hepatocellular carcinoma. Hepatobiliary Surg Nutr. 2014;3:98–101.

38. Cho Y, Cho EJ, Lee JH, Yu SJ, Kim YJ, Kim CY, et al. Hypoxia enhances tumor-stroma crosstalk that drives the progression of hepatocellular carcinoma. Dig Dis Sci. 2016;61:2568–77.
39. Utsunomiya T, Shimada M, Imura S, Morine Y, Ikemoto T, Mori M. Molecular signatures of noncancerous liver tissue can predict the risk for late recurrence of hepatocellular carcinoma. J Gastroenterol. 2010;45:146–52.
40. Tsuchiya M, Parker JS, Kono H, Matsuda M, Fujii H, Rusyn I. Gene expression in nontumoral liver tissue and recurrence-free survival in hepatitis C virus-positive hepatocellular carcinoma. Mol Cancer. 2010;9:74.
41. Yoo JE, Kim YJ, Rhee H, Kim H, Ahn EY, Choi JS, et al. Progressive enrichment of stemness features and tumor stromal alterations in multistep hepatocarcinogenesis. PLoS One. 2017;12:e0170465.
42. Röper K, Corbeil D, Huttner WB. Retention of prominin in microvilli reveals distinct cholesterol-based lipid micro-domains in the apical plasma membrane. Nat Cell Biol. 2000;2:582–92.
43. Kosodo Y, Röper K, Haubensak W, Marzesco AM, Corbeil D, Huttner WB. Asymmetric distribution of the apical plasma membrane during neurogenic divisions of mammalian neuroepithelial cells. EMBO J. 2004;23:2314–24.
44. Corbeil D, Röper K, Fargeas CA, Joester A, Huttner WB. Prominin: a story of cholesterol, plasma membrane protrusions and human pathology. Traffic. 2001;2:82–91.
45. Fan L, He F, Liu H, Zhu J, Liu Y, Yin Z, et al. CD133: a potential indicator for differentiation and prognosis of human cholangiocarcinoma. BMC Cancer. 2011;11:320.
46. Fako V, Martin SP, Pomyen Y, Budhu A, Chaisaingmongkol J, Franck S, et al. Gene signature predictive of hepatocellular carcinoma patient response to transarterial chemoembolization. Int J Biol Sci. 2019;15:2654–63.
47. Tang Y, Wu Y, Xue M, Zhu B, Fan W, Li J. A 10-gene signature identified by machine learning for predicting the response to transarterial chemoembolization in patients with hepatocellular carcinoma. J Oncol. 2022;2022:3822773.
48. Ye F, Jing YY, Guo SW, Yu GF, Fan QM, Qu FF, et al. Proliferative ductular reactions correlate with hepatic progenitor cell and predict recurrence in HCC patients after curative resection. Cell Biosci. 2014;4:50.
49. Moreira AJ, Rodrigues GR, Bona S, Fratta LX, Weber GR, Picada JN, et al. Ductular reaction, cytokeratin 7 positivity, and gamma-glutamyl transferase in multistage hepatocarcinogenesis in rats. Protoplasma. 2017;254:911–20.
50. Chen YL, Lin PY, Ming YZ, Huang WC, Chen RF, Chen PM, et al. The effects of the location of cancer stem cell marker CD133 on the prognosis of hepatocellular carcinoma patients. BMC Cancer. 2017;17:474.

SUPPORTING INFORMATION

Additional supporting information can be found online in the Supporting Information section at the end of this article.

How to cite this article: Kim M, Hui KM, Shi M, Reau N, Aloman C. Differential expression of hepatic cancer stemness and hypoxia markers in residual cancer after locoregional therapies for hepatocellular carcinoma. Hepatol Commun. 2022;6:3247–3259. https://doi.org/10.1002/hep4.2079